Engineering Science and Technology, an International Journal 56 (2024) 101761

Contents lists available at ScienceDirect

Engineering Science and Technology, an International Journal

journal homepage: www.elsevier.com/locate/jestch

Full Length Article

High-gain mmWave shorted rectangular ring antenna with complementary segmented-cavity backed structure

Junhyuk Cho [a], Jong-Sik Min [b], Han Lim Lee [a,b,*]

[a] School of Electrical and Electronics Engineering, Chung-Ang University, Seoul 06974, South Korea
[b] Department of Intelligent Semiconductor Engineering, Chung-Ang University, Seoul 06974, South Korea

ARTICLE INFO

Keywords:
High gain antenna
Low-profile antenna
Microstrip antenna
mmWave antenna
Planar patch antenna

ABSTRACT

An efficient gain-enhancement technique for millimeter wave (mmWave) planar patch antennas (PPAs) using a novel slot-loaded and segmented-cavity backed structure is newly proposed in this study. By incorporating a main radiator with a rectangular slot and employing a muli-layered segemented-cavity, the proposed antenna design significantly increases antenna gain beyond conventional approaches. Unlike traditional patch antennas or those with shorting pin structures, our gain-enhanced PPA utilizes the rectangular slot to electrically expand the radiation aperture, while the addition of substrate integrated pillars acorss multiple segmented ground layers markedly improves antenna directivity. The strategric use of a segmented cavity not only facilitates flexible impedance matching but also ensures consistent performance within the n257 band, accompanied by minimal gain variation. To verify the gain enhancement from the conventional patch, the proposed antenna was fabricated with a size of 1.03 $\lambda_0 \times 1.03\ \lambda_0 \times 0.1\ \lambda_0$ at 28 GHz. The measured 10-dB impedance bandwidth was 12.14 % with a maximum measured gain of the 11.28 dBi at 28 GHz. Compared to the measured gain of the conventional PPA with the same size, the gain was 39.6 % higher, which represents the highest gain per total antenna volume observed for a single PPA in the mmWave spectrum for high-gain applications, to the best of our knowledge.

1. Introduction

To satisfy the rapidly increasing demand for data, ultra-low latency and high-capacity communications, mmWave integrated devices and systems are pivotal in advancing next-generation wireless applications. Particularly, mmWave antennas are at the forefront of technologies driving the evolution of the next-generation communications, facing unique challenges in mmWave spectrum, such as high propagation loss and atmospheric attenuation [1,2]. Relying solely on higher transmit power to extend the mmWave transmission range is impractical due to high power consumption, system complexity, and the cost of constructing a practical mmWave module. Therefore, developing more efficient antenna structures, along with high-efficiency mmWave transceivers, is essential to fully harness the potential of mmWave applications [3]. The simplest and most practical solution to overcome high propagation loss and ensure clear line-of-sight communication is through array antennas. While large-scale sub-array antennas can achieve high directivity, they are hindered by significant insertion loss in the mmWave feed network, as depicted in Fig. 1. Additionally, array antennas must be integrated with multi-channel mmWave transceivers, necessitating planar antenna structures for mmWave modules. To achieve a specified effective isotropic radiated power with fewer antenna elements, the development of high-gain antennas is indispensable [4–6]. Various high-gain antenna structures have been proposed to overcome the losses in high-band frequencies. To address the high loss of mmWave, the substrate-integrated waveguide (SIW) has been widely used in microwave components and antenna designs owing to its low loss, high gain, and ease of integration with planar circuits [7–12]. However, SIW structures typically require extra layers to form cavities, often entailing multi- layered loss fabrication and increased ground size. Moreover, the dielectric in SIW-based feed networks adversely affects radiation efficiency.

To further reduce losses, gap waveguide structures [13] are being employed, but their fabrication complexity and bulkier total structure are notable drawbacks. Additionally, artificial magnetic conductor (AMC) structures beneath the antenna are utilized to attain high gain and wideband performance [14], though this method demands a larger ground size relative to the antenna size. Another approach for gain

* Corresponding author.
E-mail address: hanlimlee@cau.ac.kr (H.L. Lee).

https://doi.org/10.1016/j.jestch.2024.101761
Received 12 March 2024; Received in revised form 11 June 2024; Accepted 1 July 2024
Available online 12 July 2024
2215-0986/© 2024 Karabuk University. Publishing services by Elsevier B.V. This is an open access article under the CC BY-NC-ND license (http://creativecommons.org/licenses/by-nc-nd/4.0/).

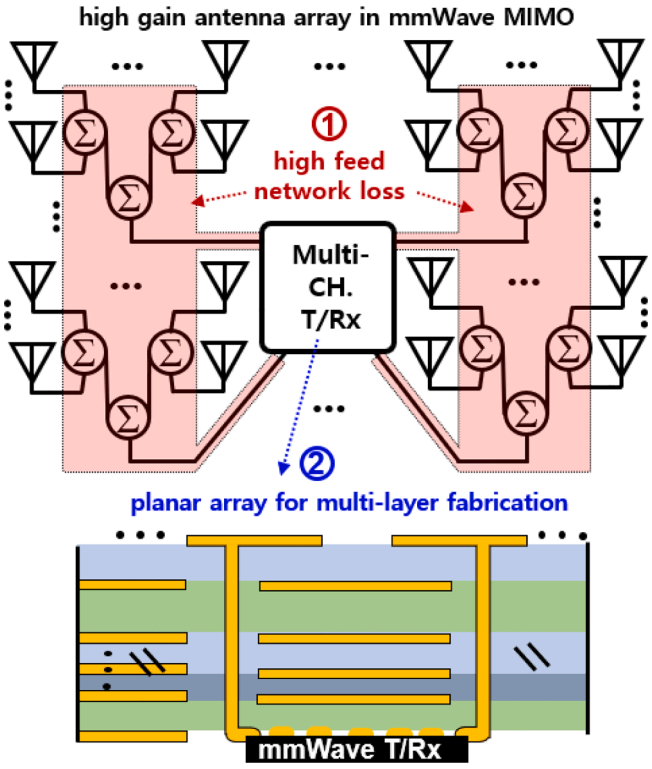

Fig. 1. mmWave antenna module considering both high feed network loss and practical fabrication.

enhancement involves employing an additional substrate with a gap above the source [15–20]. Introducing an air gap between the frequency selective surface (FSS) substrate [15,16], partially reflective surface [17], superstrate [18–20], or metasurface [21,22], and the antenna adds complexity, especially since minor alternations in the gap can significantly impact antenna performance at mmWave frequencies due to the shorter wavelengths involved. The use of horn [23,24] and dielectric resonator antenna structures [25] are also prevalent due to their excellent gain and bandwidth performance, but they tend to increase the overall height and weight of the antenna system. Moreover, employing planar sources with specific shapes [26–28] enhances antenna gain and bandwidth, but these designs may excite high-order modes or necessitate physical enlargement to alter the resonant frequency. Additionally, these techniques can be configured in an array configuration, complementing each gain or bandwidth-enhancement method, or to achieve gain flatness [29–33]. However, this strategy introduces challenges such as the need for a larger ground size for the feed network and increased losses in the feed network. Consequently, we propose a novel mmWave planar high-gain antenna structure to reduce the number of antenna elements and network loss, without resorting to extra superstrates, metallic cavities, or parasitic patches. Our design utilizes a slot-loaded and segmented-cavity-backed structure, as detailed in Fig. 2, to serve the n257 band adopted for mmWave 5G communications in South Korea, Japan, and North America.

2. Design and analysis of the proposed antenna

In the exploration of the proposed antenna design, this discussion delves into the impact of alterations in the antenna's length (L) and width (W) on its beamwidth, with a particular focus on high-gain antennas. The radiation pattern of planar patch antenna can be expressed in terms of the patch size as follows [34],

$$E_\theta = E_0 \cos\varnothing f(\theta,\varnothing) \tag{1}$$

$$E_\varnothing = -E_0 \cos\theta \sin\varnothing f(\theta,\varnothing) \tag{2}$$

where,

$$f(\theta,\varnothing) = \frac{\sin\left[\frac{\beta W}{2}\sin\theta\sin\varnothing\right]}{\frac{\beta W}{2}\sin\theta\sin\varnothing}\cos\left(\frac{\beta L}{2}\sin\theta\cos\varnothing\right) \tag{3}$$

and

$$\beta = \frac{\lambda}{2\pi} \tag{4}$$

Eqs. (1) and (2) denote the electric field intensity E, with θ representing the elevation angle and $\varnothing$ the azimuth angle. Eq. (3) models the electric field variation as influenced by direction, incorporating β as the free-space phase constant (4), W as the physical width, and L as the physical length of the antenna. Based on these equations, we derive the radiation pattern formulas for both the E-plane and H-plane,

$$F_E(\theta) = \cos\left(\frac{\lambda L}{4\pi}\sin\theta\right),\ \mathrm{E-plane},\ \varnothing = 0^\circ \tag{5}$$

$$F_H(\theta) = \cos\theta\frac{\sin\left[\frac{\lambda W}{4\pi}\sin\theta\right]}{\frac{\lambda W}{4\pi}\sin\theta},\ \mathrm{H-plane},\ \varnothing = 90^\circ \tag{6}$$

Increasing L results in a more focused E-plane radiation pattern, as evidenced by the rapid oscillation of the cosine function at $\varnothing = 0^\circ$ in Eq. (5). This effect is due to the increased length L of the antenna, which enhances the directivity by narrowing the main radiation lobe and suppressing side lobes. As L increases realative to the wavelength λ, the cosine fucntion's input, represented as $\frac{\lambda L}{4\pi}\sin\theta$, sweeps througth its periodic cycle more swiftly. This resutls in a more confined radiation pattern, evidenced by tighter beamwidth and higher directivity, which effectively reduces the angles at which nulls, or points of minimum radiation, occur. As the antenna lengthens, these null points converge more closely, which dramatically tightens the overall beamwidth. Conversely, an increase in W leads to an expand-ed H-plane radiation pattern, due to the broadedning of the null boundaries, as illustrated in Eq. (6). The broadening effect in the H-plane arises from the increase in W, which alters the distribution of radiated power. Specifically, the sinc function's argument, $\frac{\lambda W}{4\pi}\sin\theta$, increases as W expands to λ. This change causes the radiation lobes to spread wider, thereby increasing the angular spread of radiation and resulting in a less directive, but broader radiation patter. This expansion stretches the null boundaries, denoting areas of minimal radiation, and consequently decreases the antenna's directional sharpness at broadside directions. Illustrations depict type 1 antenna as a conventional design, while type 2 antenna incorporates a shorting pin positioned symmetrically opposite the signal pin on the antenna patch, as seen in Fig. 3 (a) and (b). This pin introduces inductance into the antenna's impedance, aligning the resonance frequency with the extended physical length, thereby ensuring frequency matching at 28 GHz. This approach affords a broader physical aperture compared to conventional patches. In conventional antenna patches, such as type 1 in Fig. 3 (a), radiation occurs as current flows from the signal pin to the bottom side, generating E- and H-fields. This process, pivotal for generating the electromagnetic fields necessary for antenna functionality, is clearly depicted in Fig. 3 (b), highlighting the current flow distribution. For type 1, the XZ plane exhibited a gain of 8.07 dBi and a beamwidth of 78.8°, while the YZ plane showed 8.16 dBi and 64°. Conversely, type 2, featuring a shorting pin, demonstrated in the XZ-plane a gain of 9.24 dBi and a beamwidth of 69.9°, and in the YZ-plane, 9.24 dBi and a beamwidth of 58.4°. This enhancement in performance underscores the efficacy of shorting pin in refining the antenna's aperture, thereby optimizing both beamwidth and gain. Although applying a shorting pin increased the width, it paradoxically

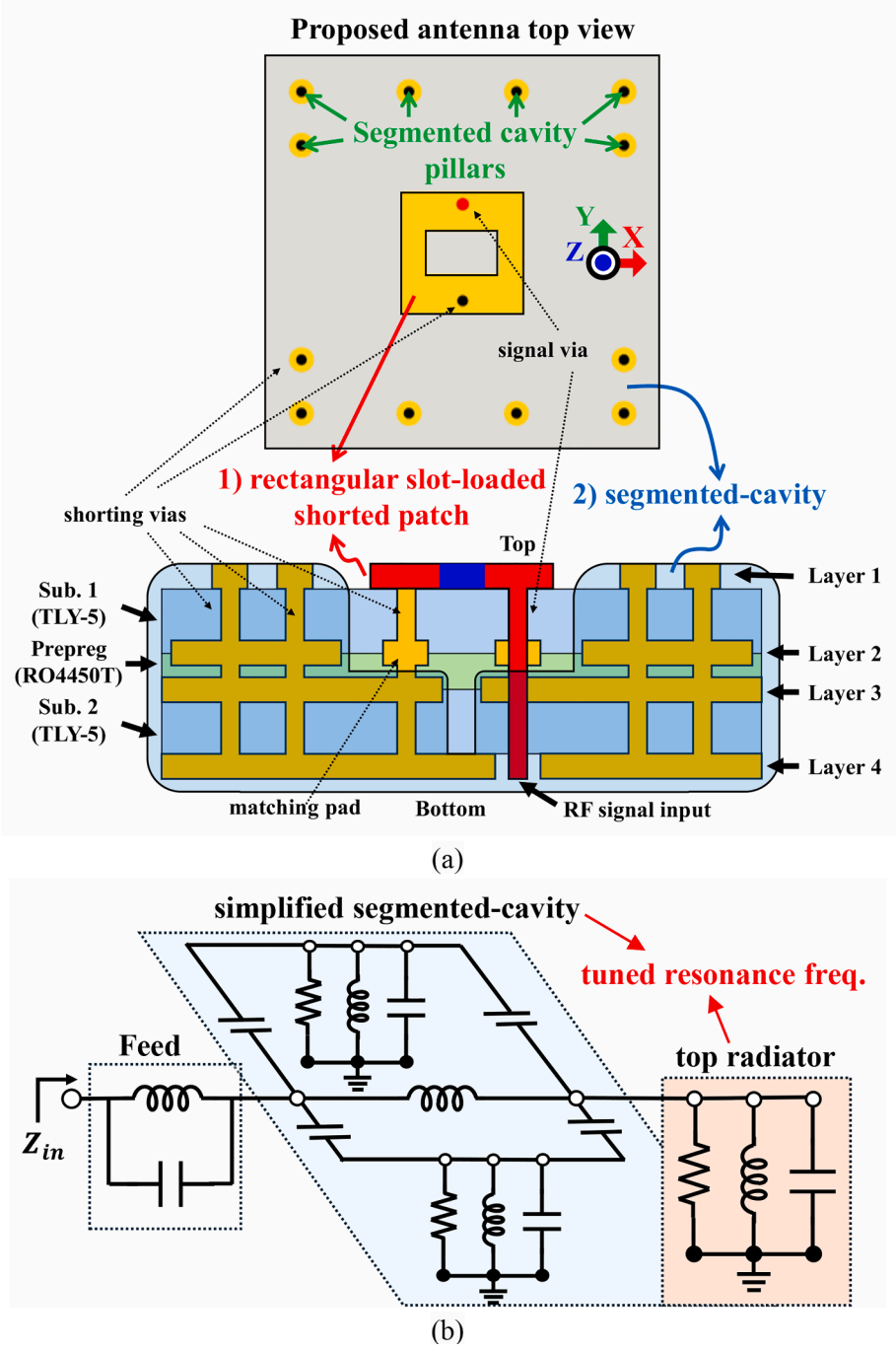

Fig. 2. Proposed antenna overview: (a) structure configuration with a rectangular slot-loaded shorted patch and multi-layer segmented cavity structures, and (b) simplified equivalent circuit model.

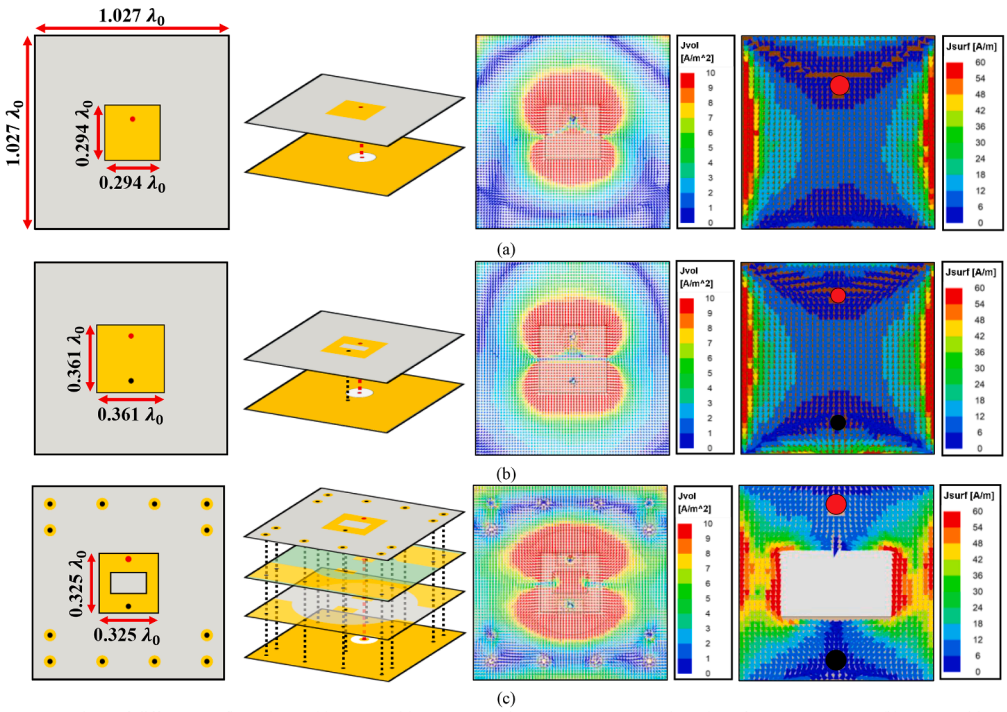

Fig. 3. Comparison of different configurations: (a) type 1 with structure, volume current vector and patch surface current vector, (b) type 2 with structure, volume current vector and patch surface current vector, and (c) type 3 with structure, volume current vector and patch surface current vector.

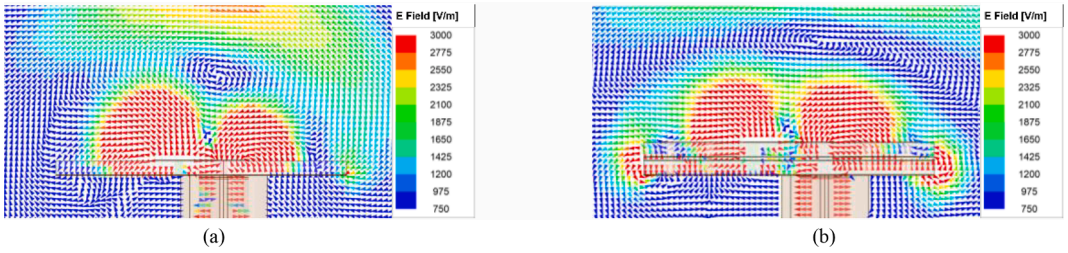

Fig. 4. E-field vector distribution in YZ-plane of (a) type 1 and (b) proposed antenna.

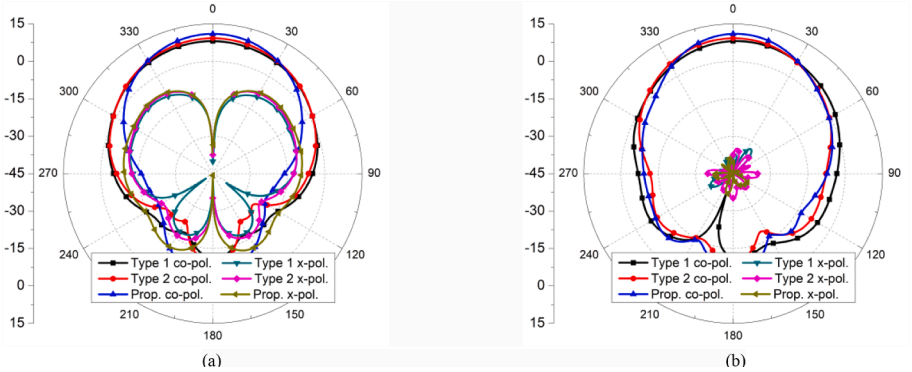

Fig. 5. Simulated beam patterns of type 1, 2 and proposed antenna in (a) XZ-plane and (b) YZ-plane.

results in a reduced beamwidth. Upon closer examination, as depicted in Fig. 3 (b) and (c), the introduction of the shorting pin not only alters the current distribution in the x-direction but also restricts the current flow. This restriction, implemented despite the increased physical width of the radiator, maintains the desired resonant frequency by effectively controlling the electrical width, thereby optimizing the beamwidth. This leads to a decrease in effective width, thus reducing the beamwidth and increasing gain, as previously discussed. Integrating slots within the antenna, as previously mentioned as slot-loaded, introduces both inductive and capacitive components. This approach increases inductance by extending the current's path through the slot, effectively augmenting the antenna's electrical length. Additionally, the square slots function as capacitors, concentrating the electric field at their edges and thereby amplifying capacitance. As demonstrated in Fig. 3 (c), the

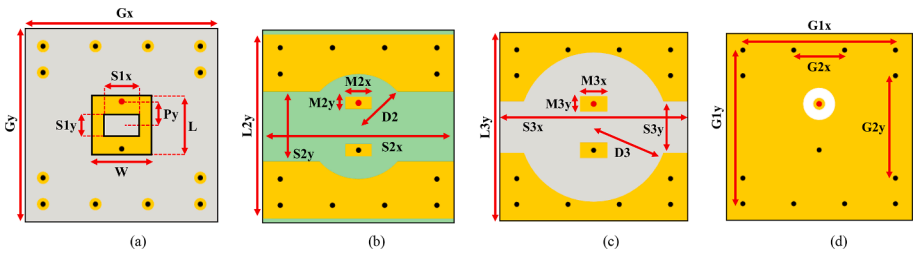

Fig. 6. Configuration of the proposed antenna's detailed layers: (a) layer 1, (b) layer 2, (c) layer 3, and (d) layer 4.

Table 1
Detailed parameter values for the proposed antenna element.

Gx	11 mm	**Py**	1.35 mm	**D2**	3 mm	**D3**	4.35 mm
Gy	11 mm	**L2y**	10.5 mm	**L3y**	11 mm	**G1x**	9 mm
W	3.4 mm	**S2x**	11 mm	**S3x**	11 mm	**G1y**	9 mm
L	3.4 mm	**S2y**	4 mm	**S3y**	3 mm	**G2x**	3 mm
S1x	2 mm	**M2x**	1.5 mm	**M3x**	1.6 mm	**G2y**	6 mm
S1y	1.2 mm	**M2y**	0.7 mm	**M3y**	0.9 mm		

addition of slots introduces additional resonance occurring along the y-direction, enabling a more compact antenna patch size while still maintaining a 28 GHz match, even with the inclusion of shorting pin. Next, the segmented cavity-back structure, characterized by its layered configuration with circular and rectangular etchings, enhanced by guide via pillars. This structured approach includes a central circular etch, supplemented by additional rectangular etchings along the x-axis. These etched layers are interconnected through via pillars, serving as a ground. The central circular etched area, connected to the ground through the pillars, centralizes the field, thereby significantly amplifying the field intensity emitted from the patch, depicted in Fig. 3 (c). The strategic configuration of layers and pillars in the rectangular etched areas along the x-direction is designed to prevent the induction of a magnetic component, which would otherwise increase the H-field on the XZ-plane and consequently broaden the beamwidth. Furthermore, as depicted in Fig. 4, unlike type 1, there is an extension of the fringing field in the E-plane, that is, the YZ-plane. This enhanced design allows the electric field to extend beyond the radiating patch in the y-direction through pillars placed laterally, leading to an extended electrical length. This increase in electrical length results in a narrower beamwidth while simultaneously increasing the gain. With the introduction of the segmented cavity-back structure in the slot-load structure, additional considerations emerge. The slot structure's current distribution around the slots is crucial. By intensifying the electric field, the cavity-back structure strengthens the current distribution around the slots and enhances the antenna's radiative gain. As a result, proposed antenna achieves an improved gain of 11.31 dBi and a reduced beamwidth of 51.2° in the XZ-plane, and 11.35 dBi and 44.8° in the YZ-plane, surpassing the performance of type 2. This improvement is evident in Fig. 5. Additionally, two elements inside the proposed antenna structure are noteworthy, and the structure of each layer and detailed dimensions can be found in Fig. 6 and Table 1. Firstly, the matching pads located at the bottom of the radiator are crucial for tuning the antenna's frequency matching, a critical component of antenna design. Their application to both the signal and shorting pins increases the inductance and capacitance, thus facilitating efficient tuning. This strategy not only maintains gain but also achieves effective matching. As depicted in Fig. 7 on the Smith chart, increases in the width (M2x and M3x) and height (M2y and M3y) of the matching pad enhance inductance and capacitance. The increase in width extends the current's path, leading to greater inductance, while a height increase not only extends the path but also enlarges the area between the patch and the matching pad, thereby increasing

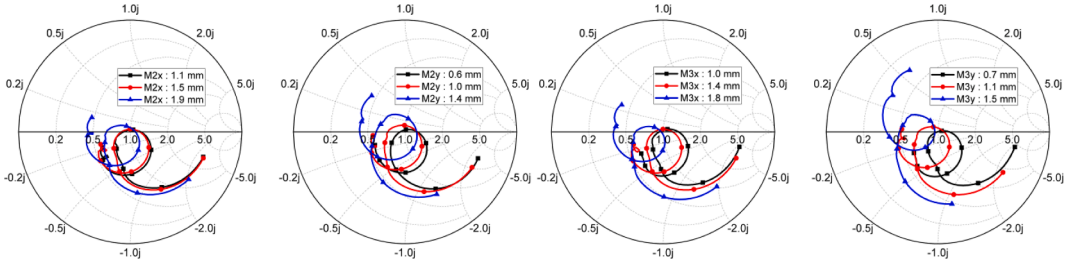

Fig. 7. Parametric analysis results for (a) M2x, (b) M2y, (c) M3x, and (d) M3y.

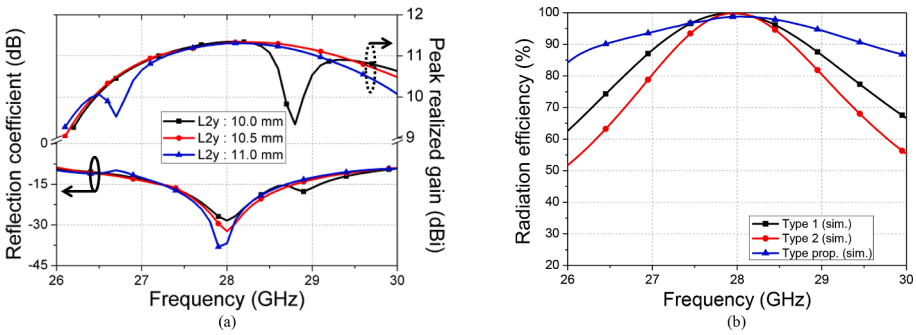

Fig. 8. Simulated (a) reflection coefficient and peak realized gain variation according to changes in L2y, and (b) radiation efficiency comparison.

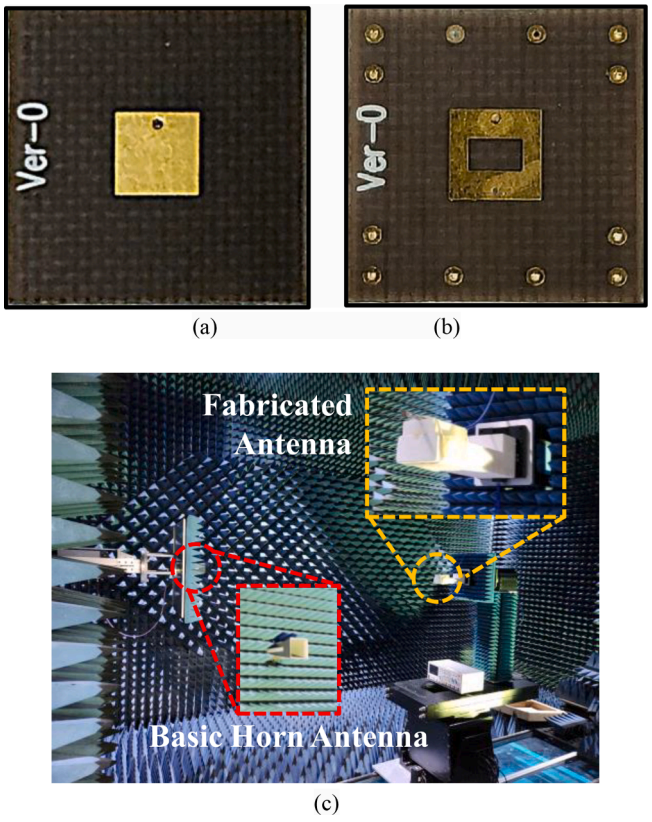

Fig. 9. Configuration of (a) reference antenna and (b) proposed antenna, and (c) measurement environment.

capacitance. These changes shift the impedance path upwards due to the increased capacitance and to the left due to the increased inductance on the chart, optimizing matching without compromising gain. Next, the L2y component plays a significant role in preserving the proposed antenna's gain flatness and continuity, as evidenced in Fig. 8 (a). The optimization of size-related discontinuity also occurs, necessitating optimization. The resulting L2y was found to be 10.5 mm. With L2y optimized, the radiation efficiency of the proposed antenna was compared to the conventional structures as shown in Fig. 8 (b). The proposed structure demonstrates more than 90 % radiation efficiency in the desired n257 band.

3. Fabrication and measurement

The performance of the proposed antenna was evaluated and compared with that of a reference antenna. For the fabrication of the proposed antenna, we utilized two Taconic TLY-5 substrates, each with a relative permittivity of 2.2, a loss tangent of 0.009, and a thickness of 0.51 *mm*. Additionally, one Rogers RO4450T substrates with a relative permittivity of 3.48, a loss tangent of 0.0031, and a thickness of 0.102 *mm* was used, resulting in a total thickness of 1.122 *mm*. The reference antenna, fabricated for comparative purposes, employed the same substrates, and is depicted in Fig. 9 (a) and (b). Both fabricated antennas were evaluated using a Keysight PNA network analyzer (N5227B), and the results is depicted in Fig. 10. For the reference antenna, the measured 10-dB bandwidth was 18.57 %, ranging from 26.2 GHz to 31.4 GHz. This measurement slightly differed from the simulation result of 19.5 %, which covered the range from 25.71 to 31.17 GHz. The measured Q-factor at the target frequency was lower than that predicted in the simulation. Conversely, for the proposed antenna, the measured 10-dB bandwidth aligned with the simulation, both showing 12.14 %, extending from 26.5 to 29.9 GHz for the measured result and from 26.23 to 29.63 GHz for the simulation. The Q-factor displayed consistency

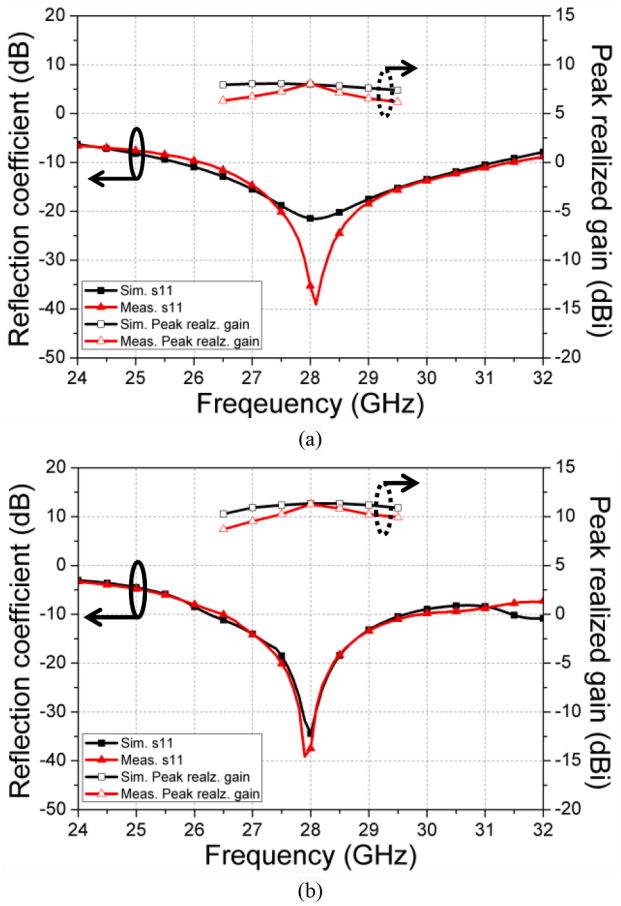

Fig. 10. Comparison of simulation and measurement results for reflection coefficient and peak realized gain for (a) the reference antenna and (b) the proposed antenna.

Antenna beam pattern and gain variation were comprehensively measured in a mmWave anechoic chamber, as depicted in Fig. 9 (c). The antennas underwent a 90° rotation to facilitate equivalent measurement conditions for both the XZ- and YZ-planes, and the measurement results are depicted in Fig. 11. Measurements for the reference antenna showed a gain of 7.95 dBi at −2° and 8.08 dBi at 7° in the XZ- and YZ-plane at the target frequency of 28 GHz. The half-power beam width (HPBW) was observed to be 56° in the XZ-plane and 44° in the YZ-plane. In contrast, simulation indicated a maximum gain to be 7.85 dBi at −1° in the XZ-direction and 7.99 dBi at 6° in the YZ-direction at 28 GHz, with the HPBW being 77.25° in the XZ-direction and 59.33° in the YZ-direction at 28 GHz.

The proposed antenna demonstrated a measured gain of 11.28 dBi at 2° in the XZ-plane and 11.26 dBi at 2° in the YZ-plane at the target frequency of 28 GHz. The HPBW was measured to be 41° in the XZ-plane and 37° in the YZ-plane, aligning closely with the simulation data, which indicated maximum gains of 11.31 dBi at 0° and 11.35 dBi at 2° in the XZ- and YZ-directions, respectively. The projected HPBW in the simulation was 51.23° in the XZ-direction and 44.83° in the YZ-direction at 28 GHz. Comparison between the measured and simulated results showed that the beamwidth was narrower in actual measurements for both cases, yet there was no notable difference in gain. Furthermore, due to the gain enhancement achieved by focusing and radiating the field towards the boresight, and adjustment in the peak gain direction was particularly observed in the YZ-directions. Regarding the simulation of cross-polarization discrimination (XPD), both the reference and proposed antennas exhibited high XPD values in the XZ-direction, exhibiting 57.91 and 51.63 at 0°, respectively. The proposed antenna showed a

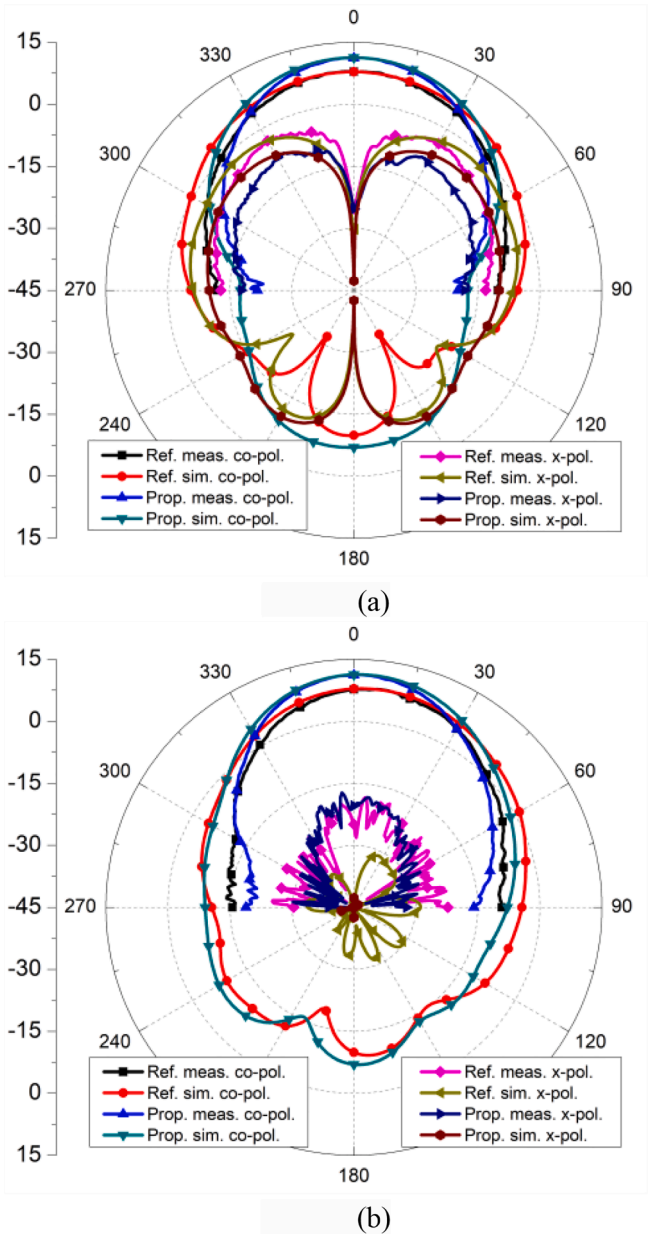

Fig. 11. Comparison of simulation and measurement results for beam pattern at 28 GHz for (a) XZ-plane and (b) YZ-plane.

4 dB lower cross-polarization than the reference antenna. In the YZ-direction, both antennas displayed lower cross-polarization compared to co-polarization, with the proposed antenna achieving higher average XPD values, though these varied across different sections. In the actual measurements, the reference antenna had an XPD of 33.13 dB at 0° in the XZ-direction, while the proposed antenna had 36.51 dB. These values were approximately 17 dB lower than the simulation results on average. However, they remained sufficiently high, maintaining the average XPD difference between the reference antenna and proposed antennas as consistent with the simulation. In the YZ-direction, contrary to the simulation results, the average XPD values of both antennas were comparable, with both showing an increased cross-polarization of around −18 dB around 0°. Despite the increased cross-polarization in the YZ-direction, the average XPD value remained a substantial 30 dB. For the simulated reference antenna, the gain variation was within 0.59 dB,

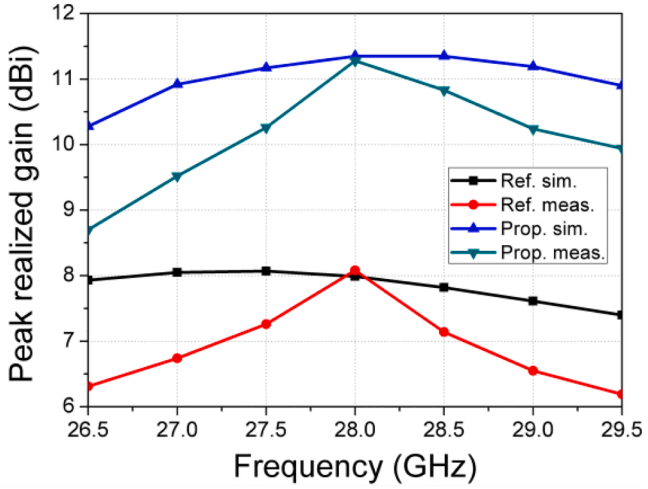

Fig. 12. Variation of peak realized gain with frequency for the reference and proposed antennas.

with a minimum gain of 7.4 dBi at 29.5 GHz, and the result is depicted in Fig. 12. In contrast, the simulated proposed antenna exhibited a gain variation within 1.07 dB, with a minimum of 10.28 dBi at 26.5 GHz. The proposed antenna showed a 3.36 dB gain difference in maximum gain, and within the 26.5 GHz to 29.5 GHz band, the gain difference between the proposed antenna and reference antenna was a minimum of 2.35 dB at 26.5 GHz, rising to a 3 dB difference from 27.24 GHz. Based on the measurement results, when assessing the gain variation within the 26.5 GHz to 29.5 GHz band centered at 28 GHz, the maximum difference was 1.89 dB at 29.5 GHz for the reference antenna and a maximum difference of 2.58 dB at 26.5 GHz for the proposed antenna. Comparing the peak gains, the minimum difference was 2.39 dB at 26.5 GHz, with more than a 3 dB were observed from 27.5 GHz to 29.5 GHz. The measurement results, especially regarding gain variation, exhibited discrepancies from the simulation results. Both the reference and proposed antennas showed consistent performance at the center frequency with the simulation results, although there was a notable reduction in gain at other frequencies. Fig. 12 indicates that the gain reduction reached up to 1.62 dB at 26.5 GHz for the reference antenna and up to 1.58 dB at 26.5 GHz for the proposed antenna, slightly higher by 0.55 dB than the simulation results. However, as also depicted in Fig. 12, both antennas displayed a similar discrepancy between the measured and simulated values. The observed gain degradation could be attributed to losses in connectors and cable lines within the measurement environment. Nevertheless, the other measurement results indicated that the discrepancy between simulation and actual results for each frequency was consistent, suggesting that the fabricated antennas' characteristics were well-preserved. Finally, Table 2 presents a comparative analysis of high-gain antennas at 28 GHz in recent years. The table highlights the compactness and high integration of the proposed antenna relative to those previously reported in this frequency range.

4. Conclusion

In this study, the gain enhancement technique for mmWave planar antenna by incorporating a slot-loaded and segmented-cavity back structure was proposed. Designed for the 26.5 GHz to 29.5 GHz band, the proposed antenna's optimized dimensions (1.03 λ_0 × 1.03 λ_0 × 0.1 λ_0) achieved a peak gain of 11.28 dBi at 28 GHz, with low gain variation in the operation bandwidth. The proposed planar structure showed the highest gain per total antenna volume without additional high-volume structures compared to other state-of-the-art antennas. It

Table 2
Comparison of the state-of-the-art mmWave High Gain antennas –.

Ref.	Antenna topology	# of antenna elements	Radiator size (λ_0^3)	Center Freq. (GHz)	10-dB Impedance Bandwidth (%)	Peak gain (dBi)	FoM (gain/ λ_0^3)
[8] / 2019	Planar	4	3.08 × 2.52 × 0.12	27.6	5.03	11.1	11.92
[14] / 2021	AMC	4	4.39 × 4.39 × 0.44	28	19.64	10	1.18
[20] / 2019	Metasurface	1	1.68 × 2.05 × 1.64	28	9.77	11.94	6.59
[24] / 2020	Clover-shaped	1	1.04 × 1.39 × 0.136	26	32.6	9	45.78
[26] / 2022	Planar	1	1.21 × 1.21 × 0.11	28	21.6	11.5	71.4
[29] / 2019	Planar	8	6.16 × 1.4 × 0.03	28	17.86	11.5	44.45
[30] / 2020	Planar	4	3.45 × 3.45 × 0.17	28	2.3	12.5	6.18
[31] / 2023	PRS	4	2.24 × 2.24 × 0.15	28	19.64	11.4	15.14
This work	Planar	1	1.03 × 1.03 × 0.1	28	12.14	11.28	106.32

outperformed a reference patch antenna of identical size and composition, showing a 3.2 dB gain enhancement. Thus, for mmWave communications or radar applications where high antenna gain can increase communication or detection ranges, the proposed design can reduce the number of antenna elements needed to achieve the required EIRP. Consequently, these advancements demonstrate the antenna's capability to overcome traditional mmWave antenna barriers in size, efficiency, and performance.

CRediT authorship contribution statement

Junhyuk Cho: Writing – original draft, Investigation. **Jong-Sik Min:** Validation, Formal analysis. **Han Lim Lee:** Writing – review & editing, Supervision, Project administration, Funding acquisition.

Declaration of Competing Interest

The authors declare that they have no known competing financial interests or personal relationships that could have appeared to influence the work reported in this paper.

Acknowledgment

This work was supported in part by Institute for Information & communications Technology Planning & Evaluation (IITP) grant funded by the Korea Government (MSIP) (No. 2018-0-00190, Development of Core Technology for Satellite Payload), and in part by the Korea Institute for Advancement of Technology (KIAT) grant funded by the Korea Government (MOTIE) (P0017011, HRD Program for Industrial Innovation).

References

[1] Y. Li, L. Kwai-Man, A,, 60-GHz Dense Patch Antenna Array, IEEE Transaction on Antennas and Propagation 62 (2) (2013) 960–963.
[2] S.K. Agrawal, S. Kapil, 5th generation millimeter wave wireless communication propagation losses dataset for Indian metro cities based on corresponding weather condition, Data Brief 23 (2019) 103564.
[3] W.A. Awan, et al., Design and Characterization of Wideband Printed Antenna Based on DGS for 28 GHz 5G Applications, Journal of Electromagnetic, Eng. Sci. 21 (3) (2021) 177–183.
[4] J. Zhang, et al., 5G Millimeter-Wave Antenna Array: Design and Challenges, IEEE Wirel. Commun. 24 (2) (2017) 106–112.
[5] I. Shayea, et al., Real Measurement Study for Rain Rate and Rain Attenuation Conducted Over 26 GHz Microwave 5G Link System in Malaysia, IEEE Access 6 (2018) 19044–19064.
[6] H. Vettikalladi, Lafond Olivier, and Himdi Mohammed, High-Efficient and High-Gain Superstrate Antenna for 60-GHz Indoor Communication, IEEE Antennas Wirel. Propag. Lett. 8 (2009) 1422–1425.
[7] W. Li, T. Xiaohong, Y. Yang, Design and Implementation of SIW Cavity-Backed Dual-Polarization Antenna Array With Dual High-Order Modes, IEEE Trans. Antennas Propag. 67 (7) (2019) 4889–4894.
[8] Jin. Huayan, et al., Integration Design of Millimeter-Wave Filtering Patch Antenna Array With SIW Four-Way Anti-Phase Filtering Power Divider, IEEE Access 7 (2019) 49804–49812.
[9] I. Serhsouh, et al., Reconfigurable SIW Antenna for Fixed Frequency Beam Scanning and 5G Applications, IEEE Access 8 (2020) 60084–60089.
[10] I.L. Paula, et al., Cost-Effective High-Performance Air-Filled SIW Antenna Array for the Global 5G 26 GHz and 28 GHz Bands, IEEE Antennas Wirel. Propag. Lett. 20 (2) (2021) 194–198.
[11] M. Asaadi, S. Abdelrazik, High-Gain Low-Profile Circularly Polarized Slotted SIW Cavity Antenna for MMW Applications, IEEE Antennas Wirel. Propag. Lett. 16 (2016) 752–755.
[12] S.-J. Park, S. Dong-Hun, P. Seong-Ook, Low Side-Lobe Substrate-Integrated-Waveguide Antenna Array Using Broadband Unequal Feeding Network for Millimeter-Wave Handset Device, IEEE Trans. Antennas Propag. 64 (3) (2015) 923–932.
[13] J. Ran, et al., High-Gain and Low-Loss Dual-Polarized Antenna Array With Reduced Sidelobe Level Based on Gap Waveguide at 28 GHz, IEEE Antennas Wirel. Propag. Lett. 21 (5) (2022) 1022–1026.
[14] A.A. Ibrahim, A.E. Ali Wael, High gain, wideband and low mutual coupling AMC-based millimeter wave MIMO antenna for 5G NR networks, Int. J. Electron. Commun. 142 (2021) 153990.
[15] M. Asaadi, Afifi Islam, and Sebak Abdel-Razik, High Gain and Wideband High Dense Dielectric Patch Antenna Using FSS Superstrate for Millimeter-Wave Applications, IEEE Access 6 (2018) 38243–38250.
[16] W. Wang, Q. Cao, Y. Zheng, Bandstop frequency-selective structures based on stepped-impedance loop resonators: design, analysis, and measurement, IEEE Trans. Antennas Propag. 67 (2) (2019) 1053–1064.
[17] W. Wang, Y. Zheng, Wideband gain enhancement of high-isolation fabry–pérot antenna array with tandem circular parasitic patches and radial gradient PRS, IEEE Trans. Antennas Propag. 69 (11) (2021) 7959–7964.
[18] O.M. Haraz, et al., Dense Dielectric Patch Array Antenna With Improved Radiation Characteristics Using EBG Ground Structure and Dielectric Superstrate for Future 5G Cellular Networks, IEEE Access 2 (2014) 909–913.
[19] M. Asaadi, S. Abdelrazik, Gain and Bandwidth Enhancement of 2 × 2 Square Dense Dielectric Patch Antenna Array Using a Holey Superstrate, IEEE Antennas Wirel. Propag. Lett. 16 (2017) 1808–1811.
[20] J.H. Kim, Ahn Chi-Hyung, and Bang Jin-Kyu, Antenna Gain Enhancement Using a Holey Superstrate, IEEE Trans. Antennas Propag. 64 (3) (2016) 1164–1167.
[21] V.M. Pepino, et al., 3-D-Printed Dielectric Metasurfaces for Antenna Gain Improvement in the Ka-Band, IEEE Antennas Wirel. Propag. Lett. 17 (11) (2018) 2133–2136.
[22] M.J. Jeong, et al., Millimeter-wave microstrip patch antenna using vertically coupled split ring metaplate for gain enhancement, Microw. Opt. Technol. Lett. 61 (10) (2019) 2360–2365.
[23] I. Agnihotri, S.K. Sharma, Design of a 3D Metal Printed Axial Corrugated Horn Antenna Covering Full Ka-Band, IEEE Antennas Wirel. Propag. Lett. 19 (4) (2020) 522–526.
[24] A. Elboushi, S. Abdelrazik, High-Gain Hybrid Microstrip/Conical Horn Antenna for MMW Applications, IEEE Antennas Wirel. Propag. Lett. 11 (2012) 129–132.
[25] Q. Lai, et al., Comparison of the Radiation Efficiency for the Dielectric Resonator Antenna and the Microstrip Antenna at Ka Band, IEEE Trans. Antennas Propag. 56 (11) (2008) 3589–3592.
[26] H. Ozpinar, Aksimsek Sinan, and Tokan Nurhan Turker, A Novel Compact, Broadband, High Gain Millimeter-Wave Antenna for 5G Beam Steering Applications, IEEE Trans. Veh. Technol. 69 (3) (2020) 2389–2397.
[27] J.-S. Park, et al., A Tilted Combined Beam Antenna for 5G Communications Using a 28-GHz Band, IEEE Antennas Wirel. Propag. Lett. 15 (2016) 1685–1688.
[28] K. Jinwoo, L.H. Lim, High Gain Planar Segmented Antenna for mmWave Phased Array Applications, IEEE Trans. Antennas Propag. 70 (7) (2022) 5918–5922.
[29] N. Yoon, S. Chulhun, A 28-GHz Wideband 2×2 U-Slot Patch Array Antenna, Journal of Electromagnetic, Eng. Sci. 17 (3) (2017) 133–137.
[30] S. Zhu, et al., A Compact Gain-Enhancement Vivaldi Antenna Array With Suppressed Mutual Coupling for 5G mmWave Application, IEEE Antennas Wirel. Propag. Lett. 17 (5) (2018) 776–779.
[31] C.-X. Mao, et al., Planar Sub-Millimeter-Wave Array Antenna With Enhanced Gain and Reduced Sidelobes for 5G Broadcast Applications, IEEE Trans. Antennas Propag. 67 (1) (2018) 160–168.
[32] Y.-J. Kim, Kim Ye-Bon, and Lee Han Lim, mmWave High Gain Planar H-Shaped Shorted Ring Antenna Array, Sensors 20 (18) (2020) 5168.
[33] J. Jung, et al., Design of High-Gain and Low-Mutual-Coupling Multiple-Input-Multiple-Output Antennas Based on PRS for 28 GHz Applications, Elecronics 12 (20) (2023) 4286.
[34] C.A. Balanis, A. Theory, Analysis and Design, 4th ed., Wiley, New Tork, NY, USA, 2016.